GEOPHYSICS, VOL. 40, NO. 3 (JUNE 1975), P. 451–472, 23 FIGS.

THE DIPOLE MAPPING METHOD

GEORGE V. KELLER,* ROBERT FURGERSON,†
C. Y. LEE,* NORMAN HARTHILL,‡ AND
C. J. JACOBSON§

In the bipole-dipole mapping method, a current field is set up by the use of a bipole current source. The current field is then studied by making measurements of electric field intensity with dipole receivers at many locations around the bipole source. The values for electric field intensity may be used to compute apparent resistivities if we assume that the earth is uniform or to compute apparent conductance if we assume that the earth resembles a conducting sheet. Maps of apparent resistivity values or apparent conductance values may be interpreted by comparing them with similar maps computed analytically for various simplified earth models. The bipole-dipole mapping method is useful mainly in locating areas where ground resistivity varies rapidly in the horizontal direction. It has found application mainly in exploration for geothermal reservoirs but also has been used for mining exploration and engineering studies, and an example of each is described.

INTRODUCTION

Over the years, a variety of electrode arrays have come into use for measuring earth resistivity. In theory, at least, the resistivity structure of the earth can be determined by randomly placing four electrodes on the surface of the earth. Two of these are used to drive current into the earth, while the other two are used to detect the voltage developed by this current. Strictly arbitrary arrangements of electrodes are used rather rarely. Instead, most resistivity surveys are carried out with either the Schlumberger or Wenner electrode arrangements, which are standard arrays that have been in use for nearly 60 years (see Keller and Frischknecht, 1966, for a description). The dipole electrode arrays, first described by Alpin (1966), have been used to a lesser extent. Keller (1966) has described an attempt to use a dipole electrode array to measure the profile of resistivity through the earth's crust. However, the results of this study indicated that dipole surveys are normally more sensitive to lateral changes in resistivity beneath the area being surveyed than to vertical changes. Risk et al (1970) took advantage of this fact by using a bipole-dipole survey to locate the lateral boundaries of a conductive region associated with a geothermal system in New Zealand. Since then, the bipole-dipole mapping method has been widely used in prospecting for geothermal systems and, to a lesser extent, in mining exploration (Furgerson, 1970) and engineering studies. Over the last several years, we have carried out almost 150 dipole mapping surveys. In this paper we shall describe the present state of the use of dipole mapping.

In dipole mapping, a current field is established by use of a pair of source electrodes that are not necessarily closely spaced, and so they

Manuscript received by the Editor March 4, 1974; revised manuscript received September 25, 1974.
*Colorado School of Mines, Golden, Colo. 80401.
†Argonaut Enterprises, Denver, Colo. 80226; formerly Colorado School of Mines, Golden, Colo.
‡Group Seven, Inc., Golden, Colo. 80401.
§Geonomics, Inc., Berkeley, Calif. 94703; formerly, Montana College of Mineral Science and Technology, Butte, Mont.

can be said to form a source "bipole." The electric field around this source is then mapped in detail with closely spaced pairs of receiver electrodes, or "dipoles." In contrast to other methods for mapping lateral resistivity variations, with the bipole-dipole mapping method the source electrodes remain fixed in location, and only the receiver electrodes are moved. Hence, variations in electric field behavior between adjacent receiver stations can be identified with changes in earth resistivity in the neighborhood of the receiver stations, rather than with earth properties at the source location or at points between the source and receiver. Basically, the dipole mapping technique resembles the equipotential surveying technique described by Heiland (1940), with the exception that values of potential difference are converted to apparent resistivity.

BASIC FORMULAS FOR THE BIPOLE-DIPOLE ARRAY

The general scheme of a dipole mapping survey is indicated in Figure 1. The primary data obtained during a survey are the voltages detected between the two sets of receiving electrodes, the current provided to the source bipole, and the various physical dimensions of the array indicated in Figure 1. These data may be converted to values of apparent resistivity by the use of several different formulas. The conventional manner of defining apparent resistivity is to consider the resistivity a homogenous and isotropic earth would have to have to provide the voltages actually observed in the real earth. In a uniform earth, current spreads out from a single point-electrode with spherical symmetry. The electric field along the surface of the earth at a distance R_1 from a single electrode through which a current I is flowing is given by

$$E_1 = \frac{\rho I}{2\pi R_1^2}, \tag{1}$$

where ρ is the resistivity of the assumed uniform earth. When two source electrodes are used instead of one, there is also a contribution to the electric field due to the current flowing from the second electrode:

$$E_2 = \frac{-\rho I}{2\pi R_2^2}, \tag{2}$$

where R_2 is the distance from the observation point to the second current electrode.

One method of computing apparent resistivity would be to consider only the component of electric field that would be detected with a dipole receiver array oriented parallel to the axis of the bipole source. The parallel electric field $E_\parallel$ can be obtained by projecting the electric fields for the two pairs of receiver electrodes onto the parallel direction. In this way, for a homogeneous earth, one finds the expression for computing apparent resistivity is

$$\rho_{a,\parallel} = \frac{2\pi R_1^2}{\left\{\cos a_1 + \left(\frac{R_1}{R_2}\right)^2 \cos a_2\right\}} \frac{E_\parallel}{I}. \tag{3}$$

Similarly, $E_\perp$ the component of electric field measured perpendicular to the source bipole may be used to define another apparent resistivity:

$$\rho_{a,\perp} = \frac{2\pi R_1^2}{\left\{\sin a_1 - \left(\frac{R_1}{R_2}\right)^2 \sin a_2\right\}} \frac{E_\perp}{I}. \tag{4}$$

Still another definition of apparent resistivity is useful, one expressed in terms of the magnitude of the electric field at a receiver station, regardless of its direction (Risk et al, 1970). The electric fields E_1 and E_2 are vector quantities, and so must be added vectorially. The vector sum is

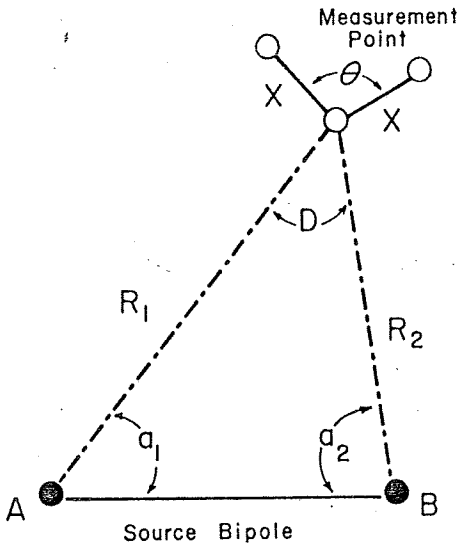

FIG. 1. Electrode layout used for bipole-dipole mapping surveys.

$$E_T = \frac{\rho I}{2\pi R_1^2}\left\{1 + \left(\frac{R_1}{R_2}\right)^4 - 2\left(\frac{R_1}{R_2}\right)^2 \cos D\right\}^{\frac{1}{2}}. \quad (5)$$

Inversion of this equation to provide a solution for ρ provides the expression for computing apparent resistivity under the assumption of spherical symmetry in current flow for a uniform earth. The expression for apparent resistivity may be written as

$$\rho_a = K_{g1} K_{g2} \frac{E_T}{I},$$

where

$$K_{g1} = 2\pi R_1^2$$

and

$$K_{g2} = \left\{1 + \left(\frac{R_1}{R_2}\right)^4 - 2\left(\frac{R_1}{R_2}\right)^2 \cos D\right\}^{-\frac{1}{2}}. \quad (6)$$

This formula is convenient for computations in the field, where a computer is not available. The first geometric factor, K_{g1}, is exactly the ideal Schlumberger array geometric factor if the distance R_1 is considered to be equivalent to half the current electrode separation in the ideal Schlumberger array (spacing between potential electrodes approaches zero). It may be calculated by use of a sliderule or portable calculator. The second geometric factor K_{g2} is more complicated to calculate in the field but may be read easily from the nomograph shown in Figure 2 once the parameters R_1/R_2 and D have been scaled from the survey base map.

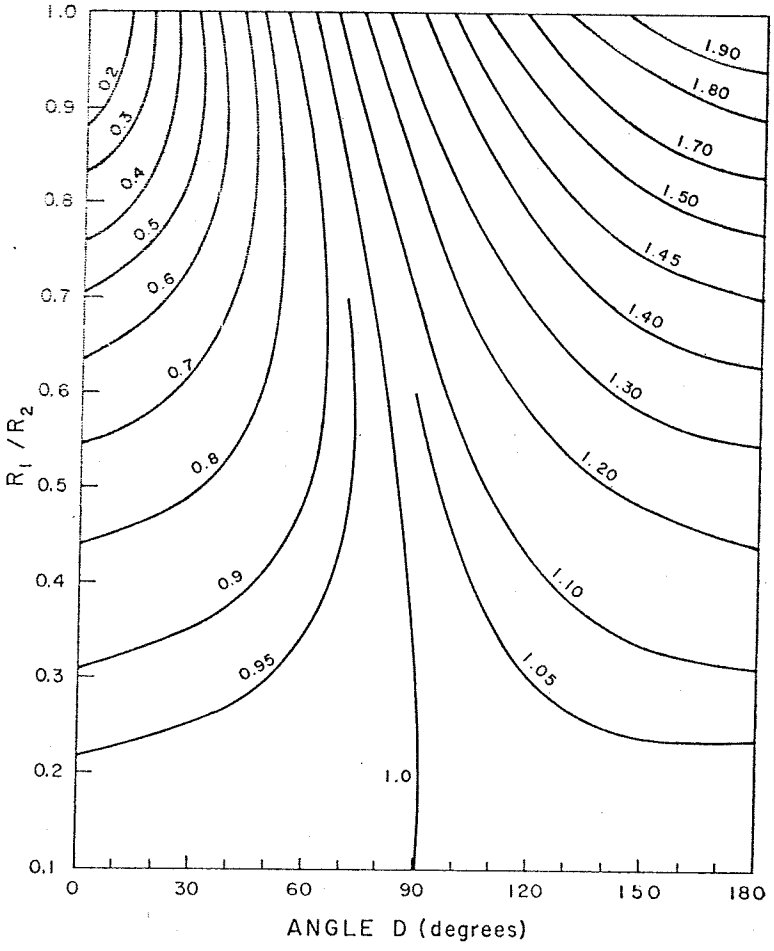

Fig. 2. Nomograph yielding values for K_{g2}, a geometric correction factor used in computing apparent resistivity from bipole-dipole data.

For many applications of the dipole mapping method, the distance from source to receiver is greater than the depth to an electrical basement of much higher resistivity than the overlying layers. When this is the case, the values of apparent resistivity will tend to increase with distance from the source and give a false impression about the nature of lateral changes in resistivity or thickness of the conductive part of the section. In this case, the computation of resistivity on the basis of an assumed spherical spreading of current seems inappropriate. We have found that a more meaningful way to reduce the field data is to use a formula based on the assumption of cylindrical spreading of current through a thin conductive plate. For current spreading in a thin plate, the electric field depends on the ratio of plate thickness to resistivity h/ρ, a quantity S which is known as the conductance of the plate. The electric field at the surface of the thin plate for a current I flowing from a single electrode is (Keller and Frischknecht, 1966)

$$E_1 = \frac{I}{2\pi S R_1}, \tag{7}$$

where R_1 is the distance from the first current electrode to the observation point. With the addition of a second electrode to complete the bipole current source, the contribution of a second electric field at the observation point must be considered:

$$E_2 = \frac{-I}{2\pi S R_2}. \tag{8}$$

The vector sum of these two electric fields is

$$E_t = \frac{I}{2\pi S R_1}\left[1 + \left(\frac{R_1}{R_2}\right)^2 - 2\left(\frac{R_1}{R_2}\right)\cos D\right]^{\frac{1}{2}}. \tag{9}$$

Solution of this equation for S provides the means for computing "apparent conductance" under the assumption of cylindrical symmetry in the spreading of current through a uniform conducting plate.

TYPE MAPS FOR DIPOLE MAPPING

Both apparent resistivity and apparent conductance are calculated for an earth which is assumed to be laterally uniform in electrical properties. This is rarely true in practice, hence it is desirable to calculate the way the apparent values for these two parameters are affected by simple models of inhomogeneous earth structures.

Layering

The mathematical expressions for the electric field about a current electrode at the surface of a horizontally stratified earth are well known. For the case of a single layer resting on a uniform substratum of infinite thickness, the electric field is (Meinardus, 1967)

$$|E| = \frac{\rho_1 I}{2\pi R^2}\int_0^\infty G(\lambda)\lambda J_1(\lambda R)\, d\lambda. \tag{10}$$

Here

$$G(\lambda) = \frac{1 - Ke^{-2\lambda h_1}}{1 + Ke^{-2\lambda h_1}};$$

$$K = \frac{\rho_2 - \rho_1}{\rho_2 + \rho_1};$$

ρ_1 and ρ_2 are the resistivities of the surface layer and substratum, respectively;
R is the distance from the source electrode to the receiver station;
h_1 is the thickness of the layer;
λ is a dummy variable of integration; and
I is the current input to the current electrode.

The electric field E is directed radially outward from the source electrode. For a bipole source the contributions from two such source electrodes must be considered.

Various methods are available for the numerical evaluation of the integral in equation (10) (Meinardus, 1967). We used a method, consisting of a Taylor series expansion of the function $G(\lambda)$ that is equivalent to considering an image series (Roman, 1959).

The dipole maps shown in Figures 3 and 4 are typical of those for a simple two-layer earth. In each case, it is assumed that a bipole of unit length is placed on the surface of an earth in which a layer of unit thickness (equal to bipole length) lies on top of an infinitely thick substratum. The dipole maps in Figure 3 were calculated for an infinitely resistive basement. The surface layer is assumed to have unit resistivity. As may be seen, the contours of apparent resistivity form peanut-shaped patterns about the source bipole, a behavior that is characteristic of layering. The ratio of length to width of the

ntours reflects the well-known fact that measurements made along the polar axis of a bipole ...ree do not detect the presence of a resistive ...sement until larger spacings are reached than ...e required when measurements are made along ...e equatorial axis (Keller, 1966). It should also ...e noted that there are two small regions about ...e ends of the bipole where the apparent re...sivity is lower than unity, the resistivity as...ned to the surface layer.

In contrast to the apparent resistivity, which ...ows large variations as a function of distance ...om the source, the apparent conductance ...ows very little change over most of the map ...fter reaching some 70 percent of the correct ...lue of S for the surface layer at a distance of ...out one unit from the bipole. If the basement ... perfectly insulating, the actual value for ...nductance of the surface layer—1 unit—is the ...aximum value obtained by the computed ap...rent value.

The patterns in Figure 4 were computed for ... layer of unit resistivity and unit thickness ...sting on an infinitely thick substratum with ... resistivity of zero. Here, both the apparent ...nductance and the apparent resistivity vary ...rongly with distance from the source. The fact ...at in this case the length to width ratio for ...ntours is closer to unity than it was in the ...se of a resistant substratum suggests that here ...e depth of penetration for measurements made ...ong the polar axis of the bipole source is more

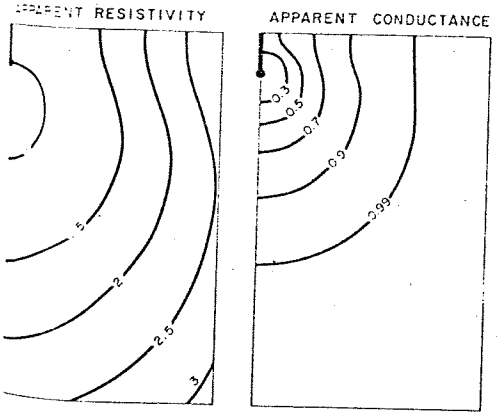

FIG. 3. Contour maps of apparent resistivity and ...pparent conductance values computed for the ...se of a single layer resting on an insulating ...asement. The bipole source has a length equal ...o the layer thickness.

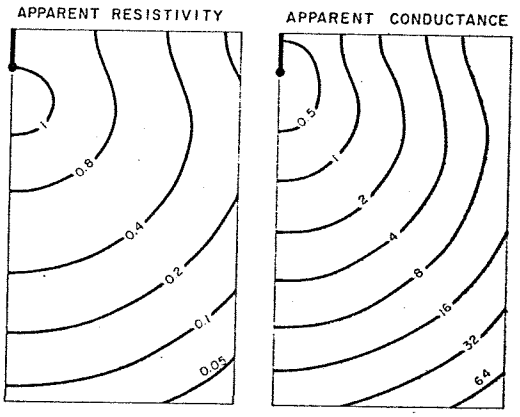

FIG. 4. Contour maps of apparent resistivity and apparent conductance values computed for the case of a single layer resting on a perfectly conducting substratum. The bipole source has a length equal to the layer thickness.

nearly the same as that for measurements made along the equatorial axis.

Dike-like structures

The case of a vertical dike is most readily evaluated by use of the image approach (Heiland, 1940; Van Nostrand and Cook, 1966; Vedrintsev, 1966; Keller and Frischknecht, 1966; and Furgerson and Keller, 1974). Figure

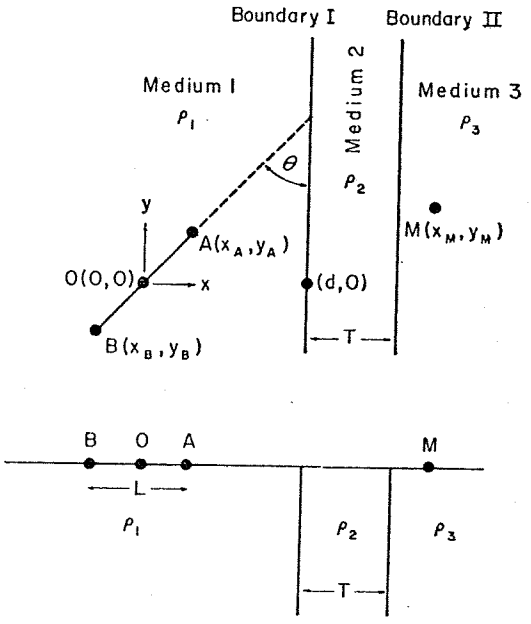

FIG. 5. Geometry of models used for computing dipole maps for vertical dike-like structures.

5 shows the geometry of the problem and defines the parameters. The dike of resistivity ρ_2 is bounded by parallel, semi-infinite, vertical contacts and has a thickness T. The media to the left and right of the dike have resistivities ρ_1 and ρ_3. The origin of coordinates is located at the center of a bipole current source of length L, consisting of electrodes A and B oriented at an angle θ to the dike. The dike is located a distance d from the origin. The electric field generated by a current I flowing in the source is measured at M.

The expression for the electric field will be different for different locations of the current electrodes and electric-field measurement points in relation to the dike. In the following equations, a superscript indicates the medium in which the current electrode is located, while subscripts indicate the medium and the direction in which the electric field is being measured. The expressions for the positive current electrode A are

$$E_{1z}^{(1)} = \frac{I\rho_1}{2\pi}\left\{\frac{\cos\beta_0}{R_0^2} + \frac{K_{12}\cos\beta_D}{R_D^2} + \sum_{n=1}^{\infty}\frac{(1-K_{12})(1-K_{21})K_{21}^{n-1}K_{23}^{n}\cos\beta_{DnT}}{R_{DnT}^2}\right\}, \quad (1$$

$$E_{1y}^{(1)} = \frac{I\rho_1}{2\pi}\left\{\frac{\sin\beta_0}{R_0^2} + \frac{K_{12}\sin\beta_D}{R_D^2} + \sum_{n=1}^{\infty}\frac{(1-K_{12})(1-K_{21})K_{21}^{n-1}K_{23}^{n}\sin\beta_{DnT}}{R_{DnT}^2}\right\}, \quad (1$$

$$E_{2z}^{(1)} = \frac{I\rho_2}{2\pi}(1-K_{12})\left\{\frac{\cos\beta_0}{R_0^2} + \sum_{n=1}^{\infty}\frac{K_{21}^{n-1}K_{23}^{n}\cos\beta_{DnT}}{R_{DnT}^2} + \sum_{n=1}^{\infty}\frac{K_{21}^{n}K_{23}^{n}\cos\beta_{TP}}{R_{TP}^2}\right\}, \quad (1$$

$$E_{2y}^{(1)} = \frac{I\rho_2}{2\pi}(1-K_{12})\left\{\frac{\sin\beta_0}{R_0^2} + \sum_{n=1}^{\infty}\frac{K_{21}^{n-1}K_{23}^{n}\sin\beta_{DnT}}{R_{DnT}^2} + \sum_{n=1}^{\infty}\frac{K_{21}^{n}K_{23}^{n}\sin\beta_{TP}}{R_{TP}^2}\right\}, \quad (1$$

$$E_{3x}^{(1)} = \frac{I\rho_3}{2\pi}(1-K_{12})(1-K_{23})\left\{\frac{\cos\beta_0}{R_0^2} + \sum_{n=1}^{\infty}\frac{K_{21}^{n}K_{23}^{n}\cos\beta_{TP}}{R_{TP}^2}\right\}, \quad (1$$

$$E_{3y}^{(1)} = \frac{I\rho_3}{2\pi}(1-K_{12})(1-K_{23})\left\{\frac{\sin\beta_0}{R_0^2} + \sum_{n=1}^{\infty}\frac{K_{21}^{n}K_{23}^{n}\sin\beta_{TP}}{R_{TP}^2}\right\}, \quad (1$$

where

$$x = x_M - x_A$$

$$y = y_M - y_A$$

$$D = d - x_A$$

$$x_A = (1/2)L\sin\theta$$

$$y_A = (1/2)L\cos\theta$$

$$K_{12} = \frac{\rho_2 - \rho_1}{\rho_2 + \rho_1} = -K_{21}$$

$$K_{23} = \frac{\rho_3 - \rho_2}{\rho_3 + \rho_2} = -K_{32}$$

$$R_0 = (x^2 + y^2)^{\frac{1}{2}}$$

$$R_D = \{(x - 2D)^2 + y\}^{\frac{1}{2}}$$

$$R_{DnT} = \{[x - 2(D + nT)]^2 + y^2\}^{\frac{1}{2}}$$

$$R_{TP} = \{(x + 2nT)^2 + y^2\}^{\frac{1}{2}}$$

$$\cos\beta_0 = \frac{x}{R_0}$$

$$\cos\beta_D = \frac{x - 2D}{R_D}$$

$$\cos\beta_{DnT} = \frac{x - 2(D + nT)}{R_{DnT}}$$

$$\cos\beta_{TP} = \frac{x + 2nT}{R_{TP}}$$

$$\sin\beta_0 = \frac{y}{R_0}$$

$$\sin\beta_D = \frac{y}{R_D}$$

$$\sin\beta_{DnT} = \frac{y}{R_{DnT}}$$

$$\sin\beta_{TP} = \frac{y}{R_{TP}}.$$

The expressions for current electrode A can used for current electrode B if the followi changes are made:

$$I \rightarrow -I$$

$$D \rightarrow d - x_B$$

$$x \rightarrow x_M - x_B$$

$$y \rightarrow y_M - y_B,$$

where

$$x_B = -(1/2)L \sin \theta$$

$$y_B = -(1/2)L \cos \theta.$$

Similar expressions can be given for $E^{(2)}$ and $E^{(3)}$, electric field components observed with the bipole source located in region 2 (the dike) or region 3 (the far side of the dike), and these are given by Furgerson and Keller (1974). We will show examples only for the case in which the bipole source is located in region 1 (the near side of the dike); we calculated these examples using the expressions given here. Values were computed for the electric field components and converted to values of apparent resistivity by use of the geometric factors defined by equation (6).

The maps shown in Figures 6–9 are typical of the maps computed for a large number of dikes with infinite vertical extent. The first two were computed for the case of a source bipole with a length equal to the width of the dike. The bipole is oriented parallel to (Figure 6) or normal to (Figure 7) a conductive dike embedded in a resistive host rock. Contour maps are shown both for values of apparent resistivity and for values of apparent conductance. Similar maps are shown in Figures 8 and 9 for the case of a resistive dike in a more conductive host rock.

The maps have a number of interesting features which might be used as guides in the interpretation of real field data. For example, it should be noted that the variations in apparent resistivity measured along profiles crossing the dike have substantially less amplitude than the

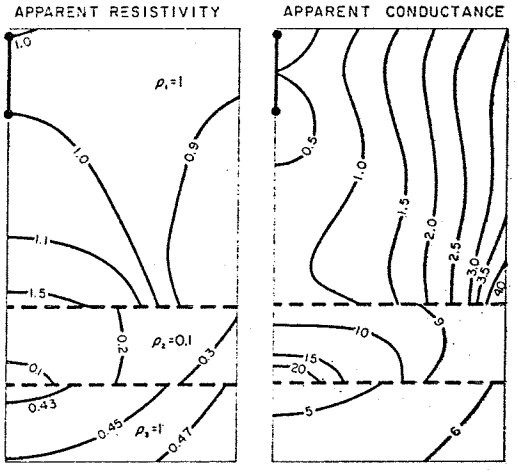

FIG. 7. Dipole maps for a vertical dike ($\rho = 0.1$) of infinite depth extent in a resistive host medium ($\rho = 1$). The source bipole is perpendicular to the dike. Dashed lines are dike contacts.

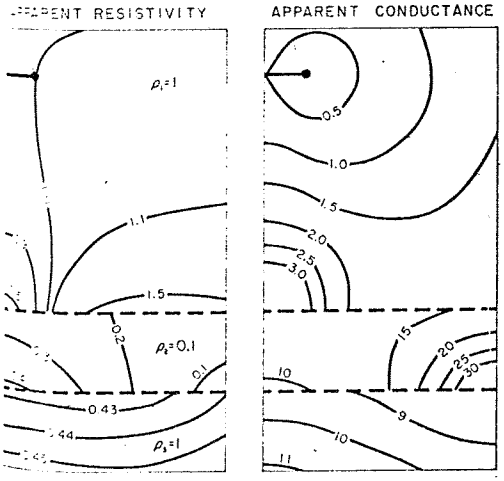

FIG. 6. Dipole maps for a vertical dike ($\rho = 0.1$) of infinite depth extent in a resistive host medium ($\rho = 1$). The source bipole is parallel to the dike. Dashed lines are dike contacts.

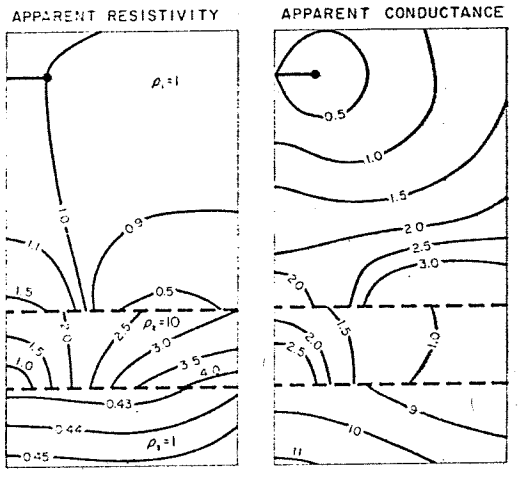

FIG. 8. Dipole maps for a vertical dike ($\rho = 10$) of infinite depth extent in a conductive host medium ($\rho = 1$). The source bipole is parallel to the dike. Dashed lines are dike contacts.

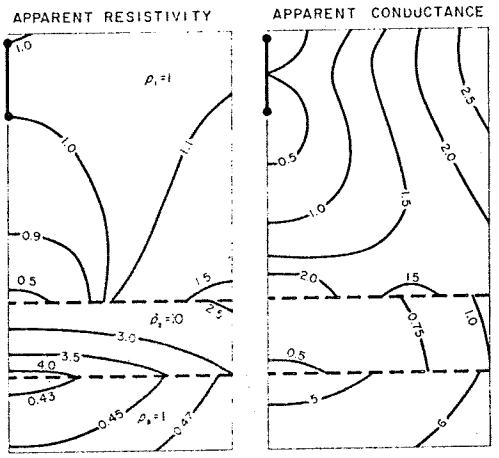

FIG. 9. Dipole maps for a vertical dike ($\rho = 10$) of infinite depth extent in a conductive host medium ($\rho = 1$). The source bipole is perpendicular to the dike. Dashed lines are dike contacts.

contrast in true resistivity between the dike and the host rock. Despite this, it appears from these maps that there should be little difficulty in recognizing the presence of either the resistive or the conductive dike. A particularly interesting feature of these two maps is that the values and patterns of apparent resistivity observed on the opposite side of the dike from the source are identical for both the resistive and conductive dikes. In both cases, for the models shown, the apparent resistivities are 40 to 50 percent of the values that would be observed if the dike were not present.

To model a dike penetrating a conductive layer bottomed by a resistive basement, we assume that the electric field for each current electrode can be expressed by equations (7) and (8). The equations for a dike can be used by making the following changes:

$$\rho_1 \to \frac{1}{S_1}$$

$$\rho_2 \to \frac{1}{S_2}$$

$$\rho_3 \to \frac{1}{S_3}$$

$$K_{12} \to K_{S,12} = \frac{S_1 - S_2}{S_1 + S_2}$$

$$K_{21} \to K_{S,21} = -K_{S,12}$$

$$K_{23} \to K_{S,23} = \frac{S_2 - S_3}{S_2 + S_3}$$

$$K_{32} \to K_{S,32} = -K_{S,23}$$

$$R_i^2 \to R_i.$$

It must be stressed that in this development it is assumed that the thickness (h) of material above the insulating basement is everywhere thin enough for the assumption of cylindrical spreading of current to be valid. Therefore, close to the bipole source, because S is assumed to be constant and finite ($S = 1$), the resistivity of the material above basement must approach zero as $h \to 0$. Examples of dipole maps for both conductive and resistive dikes bottomed by a resistive basement at a depth shallow enough for cylindrical spreading of current to predominate are given in Figures 10 and 11. For this case, the apparent conductance maps show a simpler behavior than do the apparent resistivity maps, as might be expected. In Figure 11, one might note the presence of a conductance high along the edge of the resistive dike facing the source bipole. Such false highs may be a problem of some concern in the use of the dipole mapping method for locating areas of low resistivity.

Dipping contacts

The general approach outlined by Van Nostrand and Cook (1966) and used by Lee (1973)

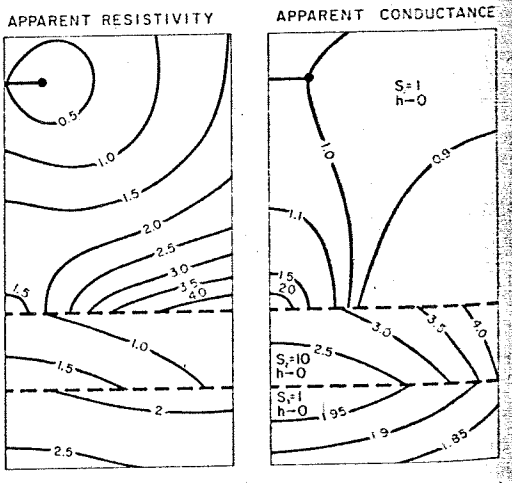

FIG. 10. Dipole maps for a vertical dike ($S = 10$) in a resistive host medium ($S = 1$). The source bipole is parallel to the dike. Dashed lines are the dike contacts. Both the dike and the host medium rest on an insulating substratum at a depth shallow enough for the assumption of cylindrical spreading of current to be valid everywhere.

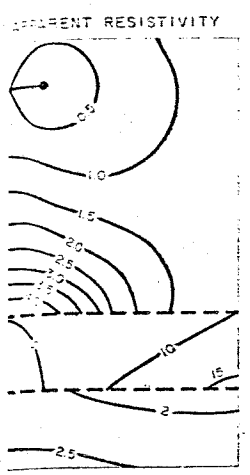

FIG. 11. Dipole maps for a
0.1) in a conductive host med
source bipole is parallel to the
are the dike contacts. Both the
medium rest on an insulating
depth shallow enough for t
cylindrical spreading of current
where.

for the dipole mapping arra
the case of a single dipping c
point source of current of s
driven into the ground thr
(Figure 12). Let the resistiv
above the contact be ρ_1 and
medium be ρ_2.

The cylindrical coordinate
most appropriate for this pr
trace of the contact is the z
such that $z = 0$ for the p
angle ϕ is such that $\phi = 0$
face to the right of the trace,
left. Let the dip of the cont
tact plane can thus be denot

The general solution to
(Van Nostrand and Cook,
form useful for the problem
is

$$U = \int_0^\infty \cos tz\, dt \int_0^\infty [A(s$$

$$+ B(s, t) \cosh s(\pi -$$

where $K_{i,s}(tr)$ is a modifi
defined by

$$K_{i,s}(u) = \int_0^\infty e^{-u \cos}$$

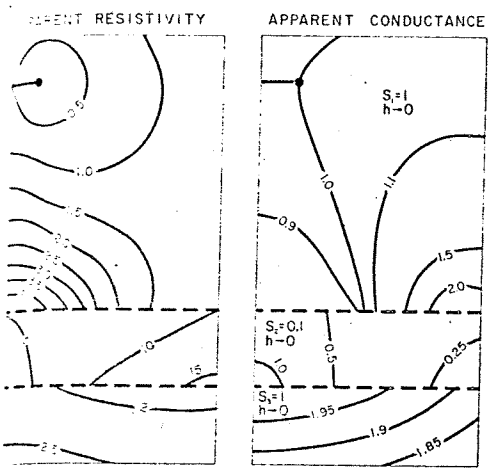

FIG. 11. Dipole maps for a vertical dike ($S = 1$) in a conductive host medium ($S = 1$). The source bipole is parallel to the dike. Dashed lines show the dike contacts. Both the dike and the host medium rest on an insulating substratum at a depth shallow enough for the assumption of cylindrical spreading of current to be valid everywhere.

The dipole mapping array is used here for the case of a single dipping contact. Consider a line source of current of strength I amperes given into the ground through electrode C (Figure 12). Let the resistivity of the medium above the contact be ρ_1 and that of the lower medium be ρ_2.

The cylindrical coordinate system (r, ϕ, z) is most appropriate for this problem. The surface trace of the contact is the z-axis. The origin is such that $z = 0$ for the point source C; the angle ϕ is such that $\phi = 0$ for the earth's surface to the right of the trace, and $\phi = \pi$ to the left. Let the dip of the contact be α; the contact plane can thus be denoted by $\phi = \alpha$.

The general solution to Laplace's equation (Van Nostrand and Cook, 1966, p. 69), in a form useful for the problem under consideration,

$$U = \int_0^\infty \cos tz\, dt \int_0^\infty [A(s, t) \cosh s(\pi + \phi) + B(s, t) \cosh s(\pi - \phi)] K_{is}(tr)\, ds,$$

where $K_{is}(tr)$ is a modified Bessel function defined by

$$K_{is}(u) = \int_0^\infty e^{-u \cosh t} \cos st\, dt.$$

u is an arbitrary argument; s and t are dummy variables, with the dimensions of inverse distance, which are introduced in the solution of Laplace's equation; and A and B are arbitrary constants, which can be evaluated by applying the appropriate boundary conditions. Therefore,

$$U_1 = \frac{I\rho_1}{2\pi}\left\{\frac{1}{R} + \frac{4k}{\pi^2}\int_0^\infty \cos tz\, dt \cdot \int_0^\infty \frac{[\sinh 2s(\pi - \alpha)] \cosh s\phi}{(\sinh s\pi) - k \sinh s(\pi - 2\alpha)} \cdot K_{is}(tr_0) K_{is}(tr)\, ds\right\}$$

for medium 1, and

$$U_2 = \frac{I\rho_1}{2\pi}\left\{\frac{1}{R} + \frac{8k}{\pi^2}\int_0^\infty \cos tz\, dt \cdot \int_0^\infty \frac{(\cosh s\alpha)[\sinh s(\pi - \alpha)] \cosh s(\pi - \phi)}{(\sinh s\pi) - k \sinh s(\pi - 2\alpha)} \cdot K_{is}(tr_0) K_{is}(tr)\, ds\right\}$$

for medium 2. Here

$$R = (z^2 + r^2)^{\frac{1}{2}}, \text{ and } k = (\rho_2 - \rho_1)/(\rho_2 + 1).$$

These expressions are identical to those obtained by Skal'skaya (1948) and Maeda (1955). It is obvious that these integrals do not lend themselves well to computations, but both Skal'skaya and Maeda have demonstrated that, if the observation points are located on the surface of the earth, these equations can be reduced to a simplified form provided the dip angle is a submultiple of π.

The case of 45-degree dip—. For points on

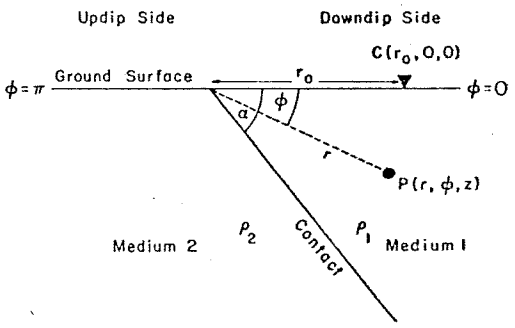

FIG. 12. Geometry of model used for an inclined plane separating media with different resistivities.

the earth's surface ($\phi = 0$), $\cosh s\phi = 1$ in medium 1, and $\alpha = \pi/4$.

$$U_1 = \frac{I\rho_1}{2\pi}\left\{\frac{1}{R} + \frac{2k}{\sqrt{r_0^2+r^2+z^2}} + \frac{k^2}{\sqrt{(r_0+r)^2+z^2}} - k(1-k^2)J(r_0, r, z)\right\}.$$

$$U_2 = \frac{I\rho_1}{2\pi}\left\{\frac{(1+k)}{R} + k(1+k)J(r_0, r, z)\right\}.$$

$$J(r_0, r, z) = \frac{1}{\sin\delta} \cdot \int_0^\infty \frac{\sinh \delta u\, du}{\sinh \pi u \sqrt{r_0^2 + r^2 + z^2 + 2r_0 r \cosh \frac{\pi u}{2}}},$$

where $\cos\delta = -k/2$, and u is a dummy variable that disappears from the expression on evaluation of the integral.

The first term in the equation for U_1 is the "normal potential" expected if the earth is homogeneous. The other terms constitute the "perturbation potential" due to the presence of the contact. Specifically, the second term can be attributed to the contribution from two electrical images of strength kI located at the points $(r_0, \pi/2, 0)$ and $(r_0, 3\pi/2, 0)$. The third term can be attributed to the contribution from an image of strength k^2I located at the point $(r_0, \pi, 0)$. The remaining term can be considered as a correction to the image solution. If the second medium is either perfectly insulating or perfectly conducting, i.e., $k = \pm 1$, the coefficients of the fourth term (the one containing the integral) vanish, and so the image solution is exact.

The case of 60-degree dip—. For points on the earth's surface and $\alpha = \pi/3$,

$$U_1 = \frac{I\rho_1}{2\pi}\left\{\frac{1}{R} + \frac{2k}{\sqrt{r^2 + r_0^2 + z^2 + r_0 r}} - \frac{2k(1-k)}{\sqrt{3-k}} \int_0^\infty \frac{\cosh \delta u\, du}{\cosh \pi u \sqrt{r_0^2 + r^2 + z^2 + 2r_0 r \cosh (2\pi/3)u}}\right\},$$

$$U_2 = \frac{I\rho_1(1+k)}{2\pi}\left\{\frac{1}{R} + \frac{k}{\sin\delta}\int_0^\infty \frac{\sinh \delta u\, du}{\sinh \pi u \sqrt{r_0^2 + r^2 + z^2 + 2r_0 r \cosh (2\pi/3)u}}\right\},$$

where $\cos\delta = (1-k)/2$.

The second term can be attributed to the contribution from two electrical images of strength kI located at $(r_0, 2\pi/3, 0)$ and $(r_0, 4\pi/3, 0)$. The remaining term is a correction to the image solution. Here again, note that if $k = 1$ an image solution to the problem is exact. If, however, $k = -1$, the image solution is inadequate. This illustrates the fact that with a perfectly conducting lower medium the dip angle must be a submultiple of $\pi/2$ if the solution based on image theory is to be exact.

The case of 90-degree dip (vertical contact)—. For points on the surface and $\alpha = \pi/2$,

$$U_1 = \frac{I\rho_1}{2\pi}\left\{\frac{1}{R} + \frac{k}{\sqrt{(r_0+r)^2+z^2}}\right\}.$$

Thus the potential in the first medium is due to the combined effects of the source and its image located at $(r_0, \pi, 0)$.

Similarly,

$$U_2 = \frac{I\rho_1(1+k)}{2\pi R},$$

where, again, R is the distance from the field point to the source point.

These last two equations are identical to those obtained by Van Nostrand and Cook (1966, p. 52–53) from an image theory solution.

Figures 13 and 14 show representative maps for total-field apparent resistivity for resistive and conductive basements, respectively, for dips of 90, 60, and 45 degrees. The effect of dip, for both positive and negative reflection coefficients, is to draw the contours closer together as the angle of dip decreases. This means that as the measuring electrodes move away from the source electrodes, the measured apparent resistivities increase or decrease more rapidly as the dip decreases. These results are in agreement with what we would expect intuitively in view of the fact that as the distance between the source and measuring electrodes becomes larger, we sample

FIG. 13. Contour
case of a source bipole
line is the contact. Ea

deeper and deeper p
13 it is important
pronounced false l
along the strike tra
source bipole.

EXAMPLES

To date, dipole n
employed most con
geothermal reservoir
cable to any explo
lateral changes in
locate the explorati
the results of thre
made using dipole
plications to geoth
exploration, and engi

FIG. 14. Contour
the case of a source
Dashed line is the con

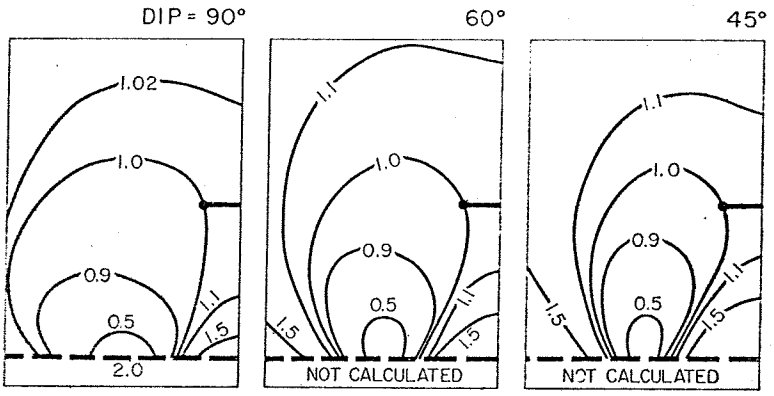

FIG. 13. Contour maps of apparent resistivity for a dipping perfectly insulating basement, for the case of a source bipole oriented parallel to the strike. Direction of dip is toward the source bipole. Dashed line is the contact. Each map is for a different dip angle as indicated.

deeper and deeper parts of the earth. In Figure 13 it is important to note the existence of a pronounced false low in apparent resistivity along the strike trace on the side facing the source bipole.

EXAMPLES OF APPLICATION

To date, dipole mapping surveys have been employed most commonly in exploration for geothermal reservoirs, but the method is applicable to any exploration problem in which lateral changes in resistivity can be used to locate the exploration target. We now present the results of three field surveys that were made using dipole mapping; they involve applications to geothermal exploration, mining exploration, and engineering studies.

Geothermal case history

A survey carried out in central Java by the Indonesian Directorate General for Power and Electricity serves as an example of the use of dipole mapping in exploration for geothermal reservoirs (Zen, 1971). The area surveyed was the Dieng Mountains, an area that had been selected as having potential geothermal resources on the basis of a study by a UNESCO Volcanological Mission in 1964 (Tazieff et al, 1966).

The Dieng Mountains are located in central Java, 65 km south of Semarang. According to Muffler (1970), the Dieng Mountains are a complex of late Quaternary volcanic vents that lie at the junction of two major topographic lineaments, a mountain range extending 50 km due west from the Dieng Mountains to the

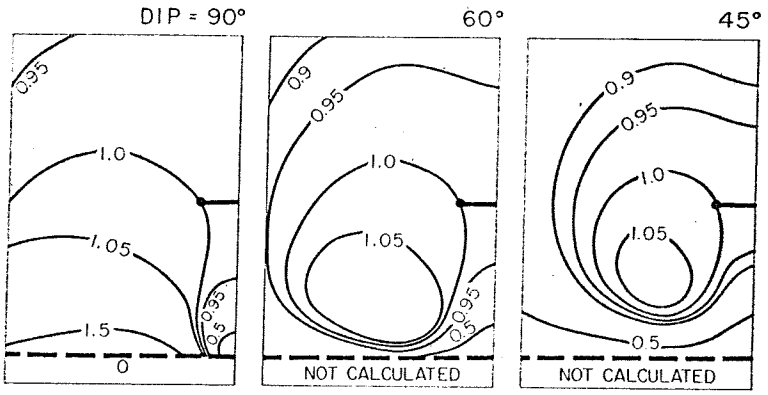

FIG. 14. Contour maps of apparent resistivity for a dipping perfectly conducting substratum, for the case of a source bipole oriented parallel to the strike. Direction of dip is toward the source bipole. Dashed line is the contact. Each map is for a different dip angle as indicated.

historic volcano, Gunung Slamet, and a row of young volcanoes (Gunung Sundoro and Gunung Sumbing) extending southeast from the Dieng Mountains for 35 km.

According to Umbgrove (1930) and Van Padang (1936), the Dieng Mountains are not a single volcano, but comprise a complex of separate extrusions ranging in composition from early basalt through successively younger olivine andesite, augite-hypersthene andesite, hornblende andesite, to biotite andesite. Each mountain probably represents a separate extrusion, either a pyroclastic cone or a viscous lava flow.

Fumaroles and hot springs cover an area approximately 11 km by 4 km, extending northwest-southeast. This activity, along with the youth of the volcanic terrain and the presence of intersecting structural lineaments, leads to the prediction of the existence of a large geothermal reservoir at depth. Accordingly, two dipole mapping surveys were conducted, one about a bipole source located in the meadows south of the village of Dieng Kulon and the other about a bipole source placed along the Dieng-Batur road a short distance east of the village of Pekasiran (see Figure 15).

For the surveys conducted on the Dieng Plateau, source bipole lengths of 1170 and 1370 m were used. Power was provided to the source bipole from a 10 KVA motor-generator set. The 220-v, 60-hz, single-phase output of the generator was stepped up to 400 or 600 v with a transformer, rectified to form direct current, and switched to cause current to flow first one way and then the other in the line connecting the source electrodes. The periodicity of reversal of current flow was selected to be 10 or 20 sec, so that the frequencies contained in the waveform of the current would be sufficiently low to avoid problems with electromagnetic attenuation of the current field and lack of penetration caused by skin-depth effects. The current waveform was asymmetrical, with the duration of current flow in one direction being about 40 percent greater than the duration in the other direction; this procedure provided a means for assigning a polarity to the voltage

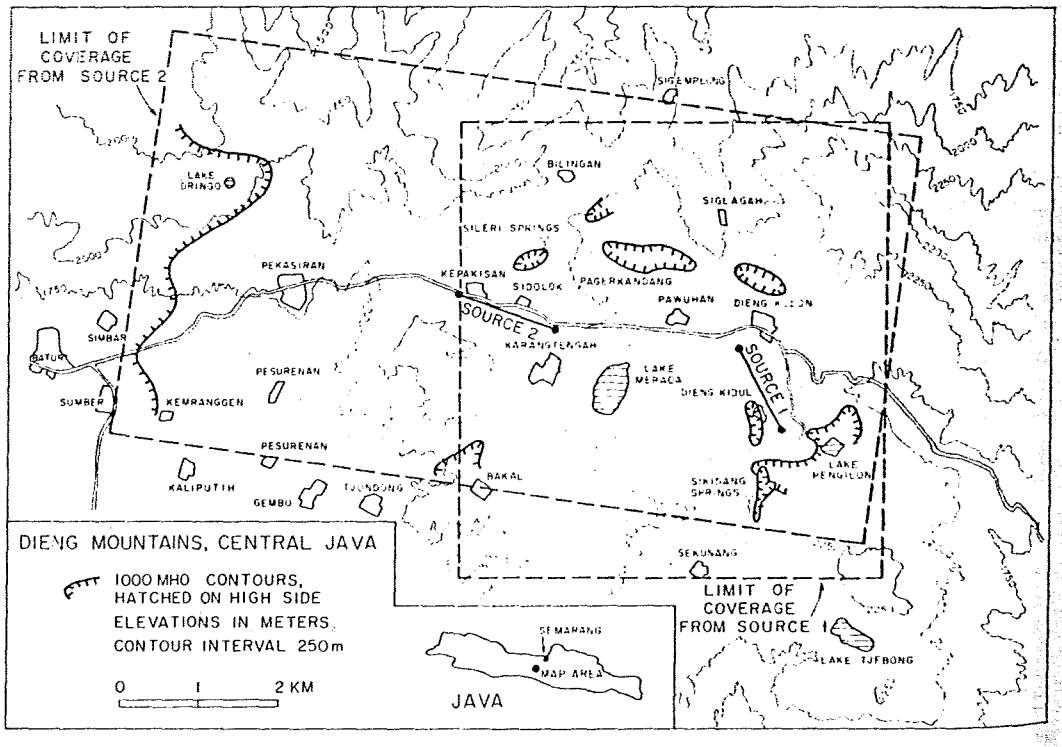

FIG. 15. Location map for a dipole mapping survey carried out in the Dieng Mountains of central Java.

detected at the receiving sites. The amplitude of the current steps was recorded graphically; current steps with amplitudes of 5 to 15 amp were used.

The current field from a source bipole was mapped by measuring voltages between electrode pairs at many points about the source bipole. The electric field is then approximated by the ratio of voltage drop to the separation between the measuring electrodes. Measurements were made with receiving electrode separations of 30 or 100 m; the longer separation was used in areas where the signal strength was low. The receiver consisted of a sensitive dc voltmeter on which the deflection due to the current reversal was measured. With the meter at its maximum sensitivity, deflections as small as 5 to 10 μv could be recognized.

Electric fields were measured at distances from the source bipole ranging up to 5 km and more. Some measurements were made within a kilometer of the ends of the source bipoles, but the principal advantage in using the dipole mapping technique lies in the utility of measurements made at distances of several kilometers from the source. At these distances, the electric field measurements typically characterize the properties of the rocks about the measurement site to depths of the order of one or two kilometers.

Almost two hundred measurements were made about each of the two source bipoles used in the Dieng Plateau survey. The computed apparent resistivity values were used to compile the contour maps of total-field apparent resistivity shown in Figures 16a and 16b. The feature of these contour maps which is of interest in terms of a geothermal system is the belt of resistivity values of less than 5 ohm-m which extends from Sileri in the northwest; along an arc through Pagerkandang, Siglagah, and the meadows south of the village of Dieng Kulon; to the hot springs and fumarole at Sikidang.

Frequently, information about the variation of resistivity with depth that is largely masked by the strong effect of lateral changes in resistivity can be extracted from dipole mapping data. In order to investigate the possibility that the depth to the base of the porous volcanic pile on the Dieng Plateau can be found from the apparent resistivity, values for each of the bipole sources were used to form resistivity sounding curves shown in Figure 17. In these compilations, the apparent resistivity values in a single quadrant are plotted as a function of distance from the near end of the source bipole. The very low resistivities associated with the anomalous belt running through the fumarole areas were not included in these compilations because they would distort the pattern in resistivity associated with changes in depth.

The three depth-sounding plots included in Figure 17 show a rapid decrease in apparent resistivity with increasing spacing for measurements made at less than one kilometer distance. This is also evident from the bird's-eye patterns at the ends of source 1 (Figure 16a), which corresponds to the patterns shown earlier for a resistive layer over a conductive basement (Figure 4). This behavior indicates that the first 200 to 300 m of rock under the Dieng Plateau has a relatively high resistivity, ranging from 50 to 200 ohm-m. High surface resistivities are a normal phenomenon in volcanic terrain; they represent the effects of low-salinity surface waters in recently formed volcanic rocks.

Two of the three depth-sounding plots show a linear increase in apparent resistivity with distance from the source for distances greater than 1.5 km. This is typical of a resistivity sounding made in an area where conductive rocks overlie a highly resistive substratum, such as crystalline basement rocks. With such a model, the apparent resistivity increases linearly with spacing for spacings greater than the depth to the resistive rock. In view of this, it would seem preferable to examine contour maps of apparent conductance values, rather than apparent resistivity values. Such maps are shown in Figures 18a and 18b.

The most direct application of the resistivity data described in the preceding sections is in delineating the boundaries of conductive areas associated with the occurrence of hot water underground. Here, the 4 ohm-m contour on the maps of apparent resistivity (or the 500 mho contour on the maps of apparent conductance) is considered to be the outermost boundary of the region where the electrical resistivity of the rock has been altered extensively by thermal activity. The main areas of thermal activity are considered to be the regions enclosed within the 2 ohm-m contour on the maps of apparent re-

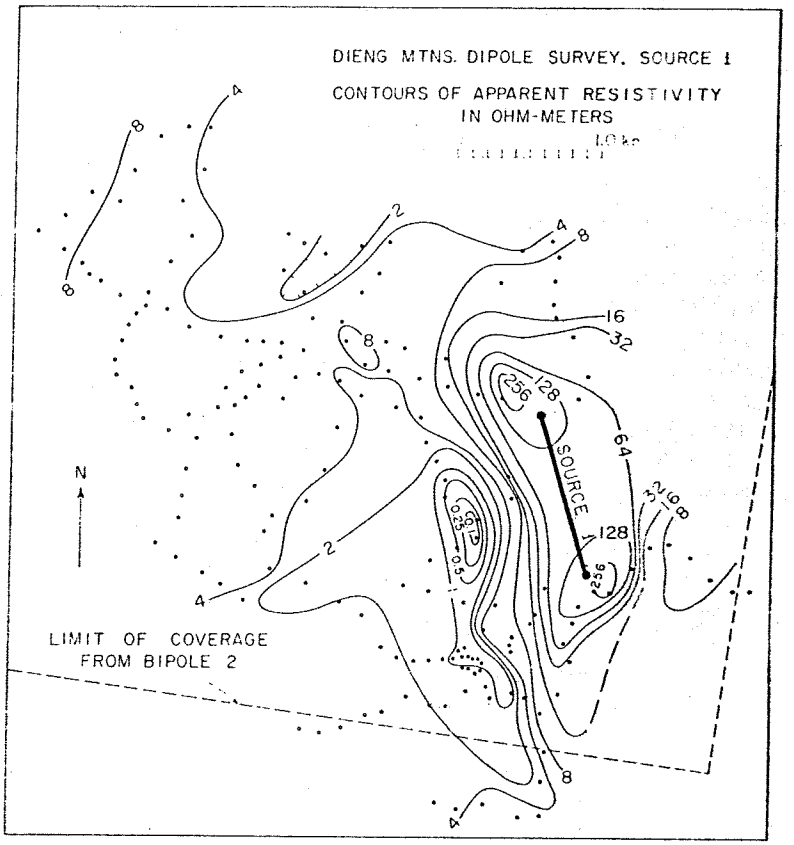

(a)

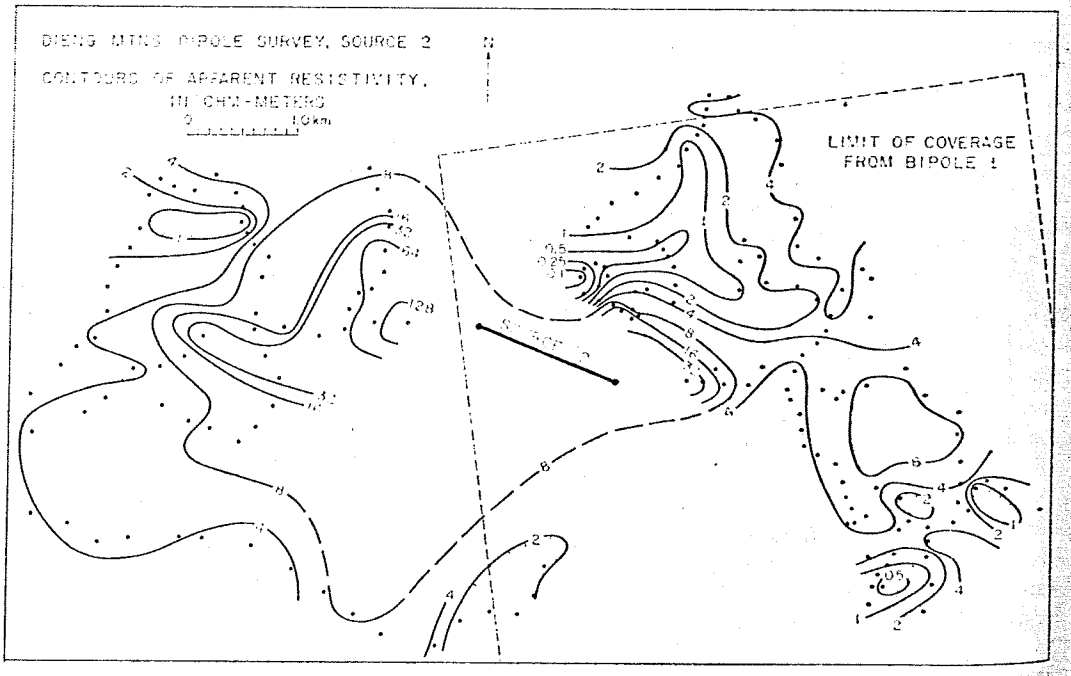

(b)

FIG. 16a and b. Contour maps of apparent resistivities measured from two bipole sources in the Dieng Mountains.

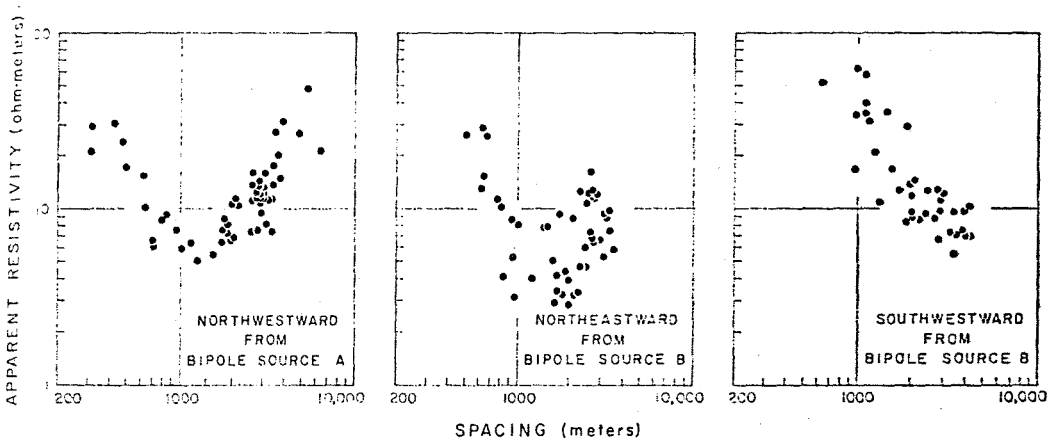

FIG. 17. Apparent resistivity values plotted as a function of distance for several groups of measurements made in the Dieng Mountains. The spacing is taken to be the distance from an observation point to the nearer end of the source bipole.

sistivity, or the 1000 mho contour on the maps of apparent conductance.

There are three such areas within the thermal belt along the eastern side of the Dieng Plateau: one centered about the Pagerkandang thermal area, one centered about the Sikidang thermal area, and a third located in and west of the meadows south of the village of Dieng Kulon. The first two areas have surface manifestations of thermal activity, but the central area has little or no surface expression.

Mining case history

A dipole mapping survey (Furgerson, 1970) was carried out in the Darwin Hills area of California, which lies in a mineral belt extending from the Inyo Mountains in the northwest to the Resting Spring district in the southeast (see location, Figure 19). The purpose of the study was to determine the geometry of the small intrusive associated with the Darwin Hills contact-metamorphic ore deposits.

Rocks in the Darwin Hills area include Paleozoic sedimentary rocks, Mesozoic plutonic and hypabyssal rocks, and Cenozoic volcanic rocks and sediments. The sequence of about 4300 m of Paleozoic rocks range in age from Early Ordovician to Permian. Dolomite is the main pre-Mississippian rock; limestone is the main younger rock.

The host rock for most of the ore deposits in the district is the Pennsylvanian and Permian Keeler Canyon formation which underlies most of the Darwin Hills. It crops out in a band about 1200 m thick along the crest and east slope of the Darwin Hills. It consists of bluish-gray limestone, silty limestone, sandy limestone, pink shale, and siltstone with much of the formation altered to calc-hornfels and tactite.

The Paleozoic rocks are intruded by the batholith of the Coso Range to the southwest, the batholith of Hunter Mountains to the northeast, and by several small plutons in the Darwin Hills and Argus Range. The Paleozoic and Mesozoic rocks are unconformably overlain by Cenozoic volcanics and sediments. Figure 19 shows the distribution of rocks and the location of the major ore bodies. The geology has been simplified, and faults are not shown.

The sedimentary rocks form a broad open syncline with an axis trending northward in Darwin Wash. The west limb of the Darwin Hills is tightly crumpled, and most of the beds are overturned with an axial plane that dips west. This is due to the intrusion of the Coso Range batholith from the southwest and the Darwin stock near the axis of the overturned syncline.

Hall and MacKevett (1962, p. 73), who did the latest geologic mapping in the area, stated that "the shape of the Darwin stock is not known, and the writers only use the term 'stock' because it has been used extensively." However, the west side of the intrusive ends in a series of sills, and a diamond drill hole extending 210 m east from the 800 level (about 180 m below the

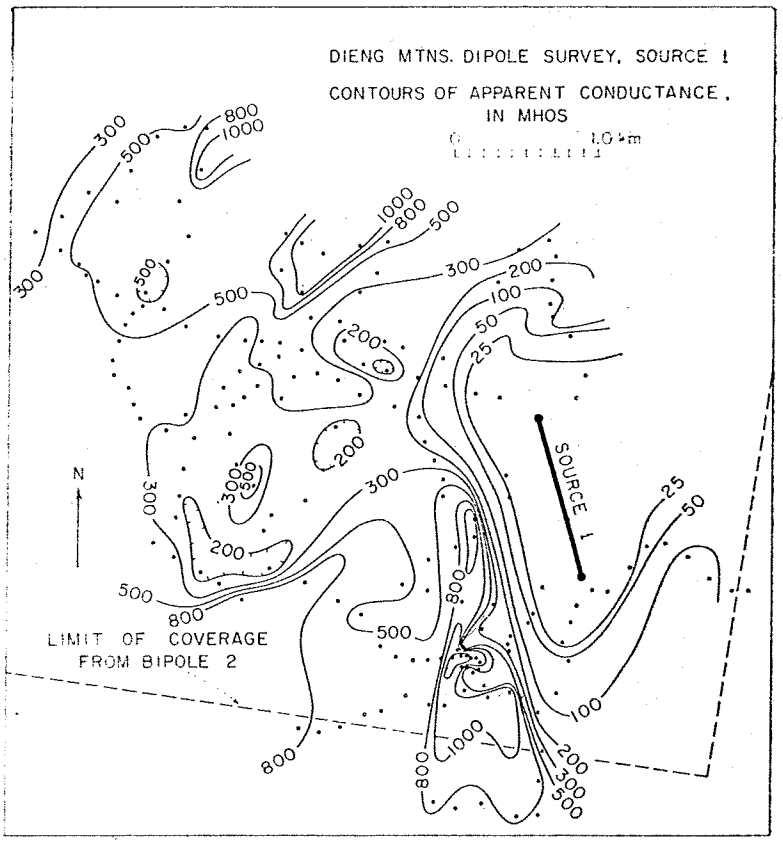

(a)

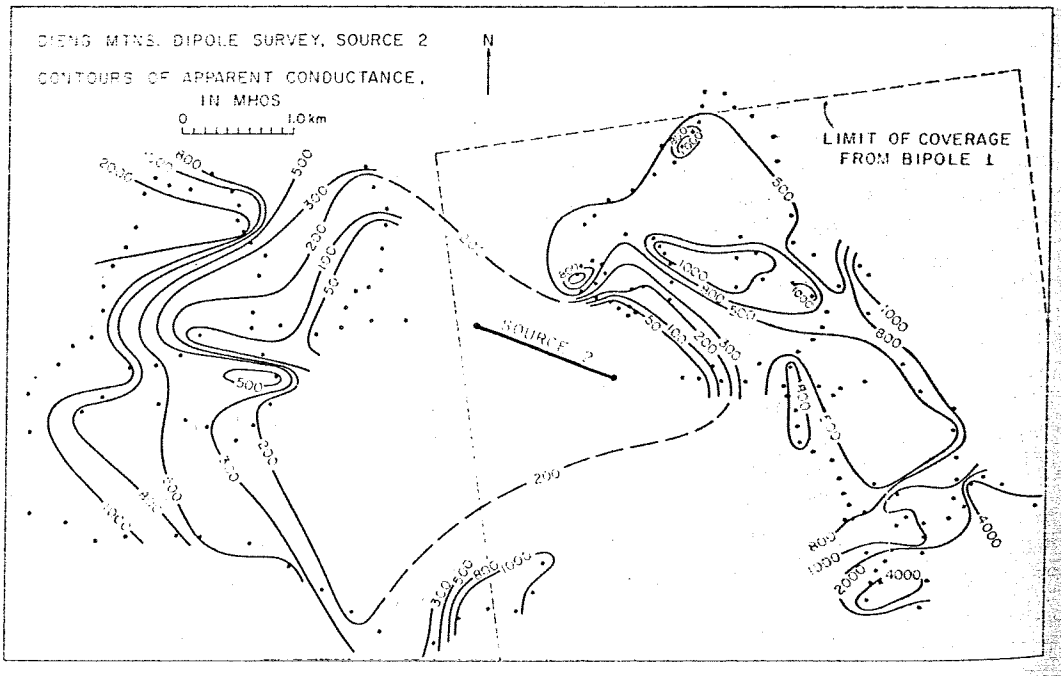

(b)

FIG. 18a and b. Contour maps of apparent conductances measured from two bipole sources in the Dieng Mountains.

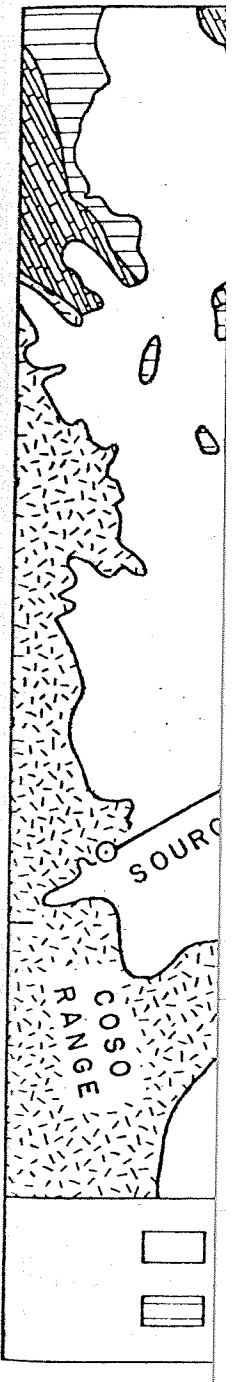

FIG. 19. Location ma

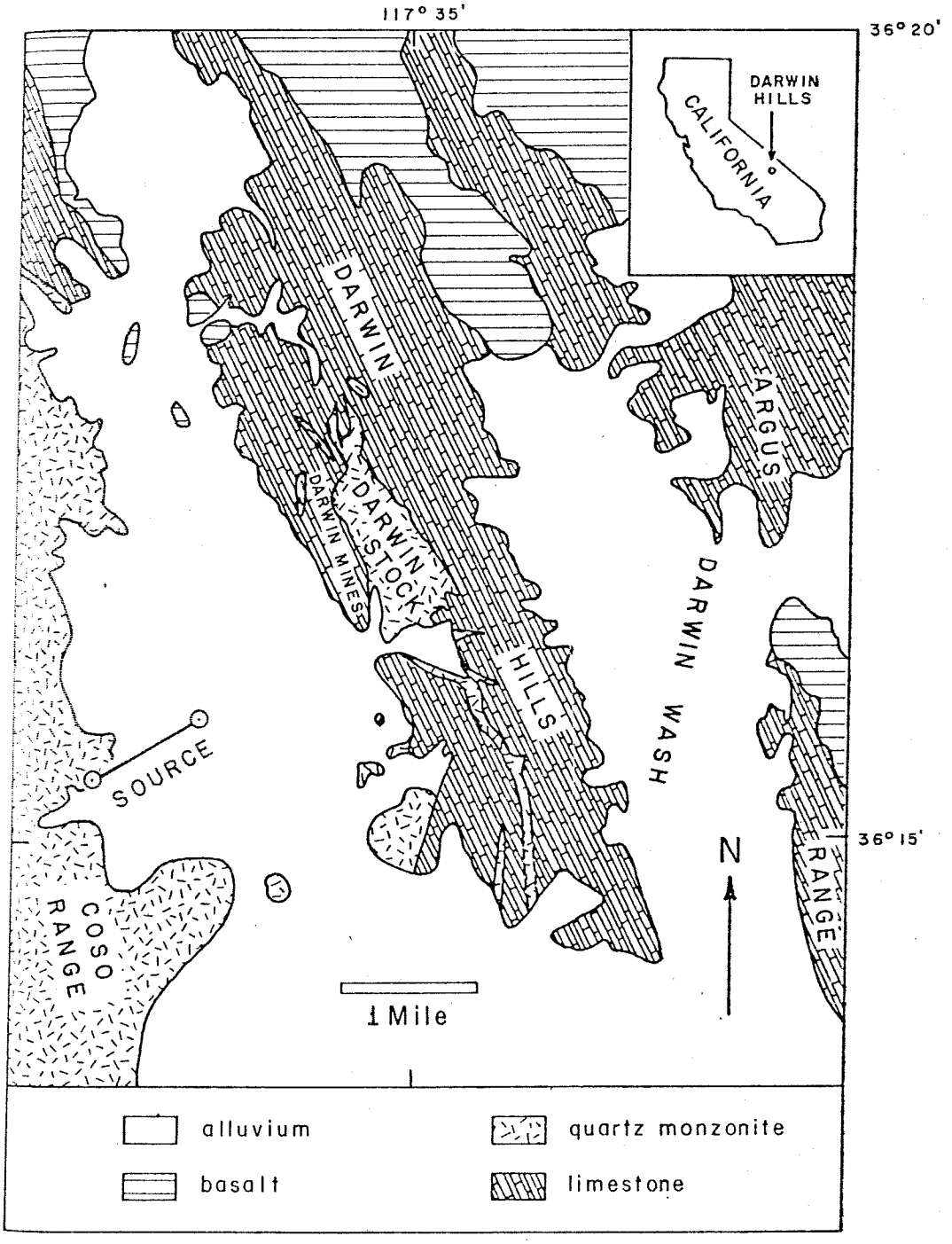

FIG. 19. Location map and simplified geologic map for a dipole mapping survey carried out in the Darwin Hills area of California.

ground-surface trace of the limestone-intrusive contact) of the Defiance workings of the Darwin mine did not cut quartz monzonite. Hall and MacKevett (1962, p. 73) use this and other evidence to suggest that "the intrusive mass may have a floor and be a laccolith."

Because most of the lead-silver-zinc deposits in the district are in Paleozoic limestone or marble close to intrusive contacts, information on the geometry of these intrusives can assist in the extension of old deposits and the exploration for new deposits.

A dipole mapping survey was carried out with source electrodes located as shown in Figure 19 to provide a source length of 1.40 km. Input currents ranged from 21 to 24 amp in the form of unidirectional square waves with a period of 70 sec. A measuring-electrode separation of 100 m was used.

Values were computed for total-field apparent resistivity at each of 55 receiver stations and are shown plotted as a contoured map in Figure 20. A plot of apparent resistivity as a function of the distance from the nearer end of the source showed no indication of the presence of a resistive basement. Therefore, the use of apparent resistivity values in preparing the contour map appears more appropriate than the use of apparent conductance.

Schlumberger and Eltran vertical electrical soundings (VES) were made at several locations to provide an indication of the resistivities of the major lithologic units. These showed that the unweathered quartz monzonite has a re-

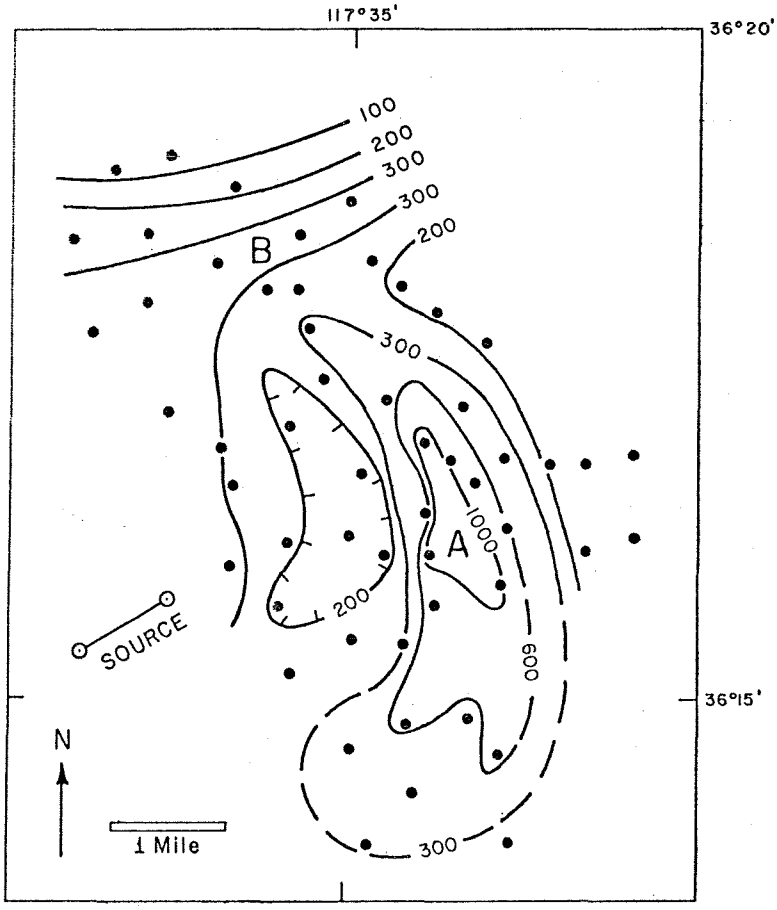

FIG. 20. Contour maps of apparent resistivity values (in ohm-meters) measured in a dipole mapping survey in the Darwin Hills.

-istivity of about 500 ohm-m, whereas the Paleozoic sediments have a lower resistivity of about 250 ohm-m. This is probably a result of the abundant faulting and fracturing caused by the emplacement of the various intrusions.

According to published geologic investigations, the contact between the quartz-monzonite of the Coso Range batholith and the limestone in the Darwin Hills runs north along the base of the Darwin Hills until it is opposite the center of the Darwin stock. From there it runs northwest and is exposed at the western edge of the map. The apparent resistivities to the west of this shallow buried contact have values from about 350 to 550 ohm-m, in the range of the modal value for the quartz-monzonite. The low on the apparent resistivity map along the axis of the bipole and extending out from the surface exposure of the Darwin stock possibly represents the deep surficial weathering observed in the Darwin stock. The total-field apparent resistivities east of the batholith-limestone contact have a background of 150 to 350 ohm-m, which is close to the modal value for the Paleozoic sediments.

Superimposed on this rather low background are two highs, included within 300 ohm-m contours, forming a pattern similar to that shown earlier in Figure 9. The large high trending north-south and marked "A" on Figure 20 is probably the nonweather resistive core of the Darwin stock. The location of the high indicates that the stock is more elongated than the surface outcrop suggests. The high trending east-west at the northern edge of the map and marked "B" on Figure 20 appears to be a nonpiercement basement high probably genetically associated with the Darwin stock. This latter high seems to merge with the Coso Range batholith to the west as suggested by the geology of Hall and MacKevett (1962, plate 1).

Engineering case history

This section describes an electrical resistivity survey carried out at Sullivan's Bend, Tenn., on January 22 and 23, 1973. The purpose of the survey was to evaluate the ultility of the dipole mapping technique as a method for rapid reconnaissance of weathered-layer physical properties in a karst limestone outcrop area. The area surveyed in Sullivan's Bend had been under consideration as a site for the construction of a power plant, and detailed foundation studies were to be made. It is reasonable to expect that where rapid or deep weathering of the limestone has taken place the weathered zone will contain more moisture than unweathered rock and that such zones will exhibit lower resistivities than unweathered rock. Thus, it is reasonable to expect a qualitative correlation between the occurrence of areas of good foundation rock and areas of relatively high resistivity in the weathered layer.

In engineering studies, survey costs are particularly important because of the great amount of detail that is required. Among the methods used was the dipole mapping method, which is rapid in application but provides only qualitative results. Such a method may be of value if it can be used to reduce the amount of work which must be done with more expensive surveying techniques such as resistivity sounding, seismic refraction surveys, and core drilling.

For the survey carried out at Sullivan's Bend, a single source bipole with a length of 320 m was used. Power was provided from a 1.5 KVA motor generator set. The 115-v, 60-hz output of the generator was switched mechanically and rectified to form direct-current steps. Each current step was approximately 10 sec long, providing time to read the voltage level at the receiver. The currents used ranged from 0.5 to 0.6 amp. The electric field around the source bipole was mapped with receiver electrode pairs at a separation of 10 m.

Apparent resistivity values computed from measurements of the total electric field are shown graphically in Figure 21, plotted as a function of the distance to the near end of the source bipole. The scatter shown by the data in Figure 21 results at least in part from lateral changes in the resistivity of either the surface weathered layer or the more resistive substrata. However, despite the scatter, the dominant tendency of the data is to increase linearly with increasing distance, a behavior which is to be expected when a conductive surface layer rests on a highly resistive substratum. If a contour map were to be prepared from values of apparent resistivity, the contours would form a roughly elliptical pattern about the source bipole. The contour patterns would reflect primarily the increase of resistivity with depth, rather than the lateral changes with which we

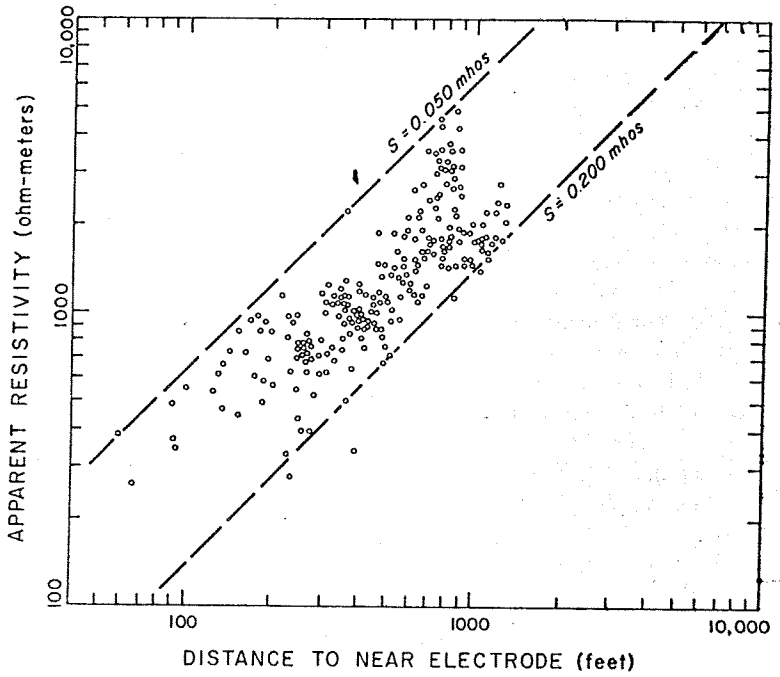

FIG. 21. Apparent resistivity values plotted as a function of the distance from the source for measurements made at Sullivan's Bend, Tenn.

are concerned. In this case, the computation of resistivity on the basis of an assumed spherical spreading of current seems inappropriate. A more meaningful way to present the field data is in terms of apparent conductance values, as shown in Figure 22.

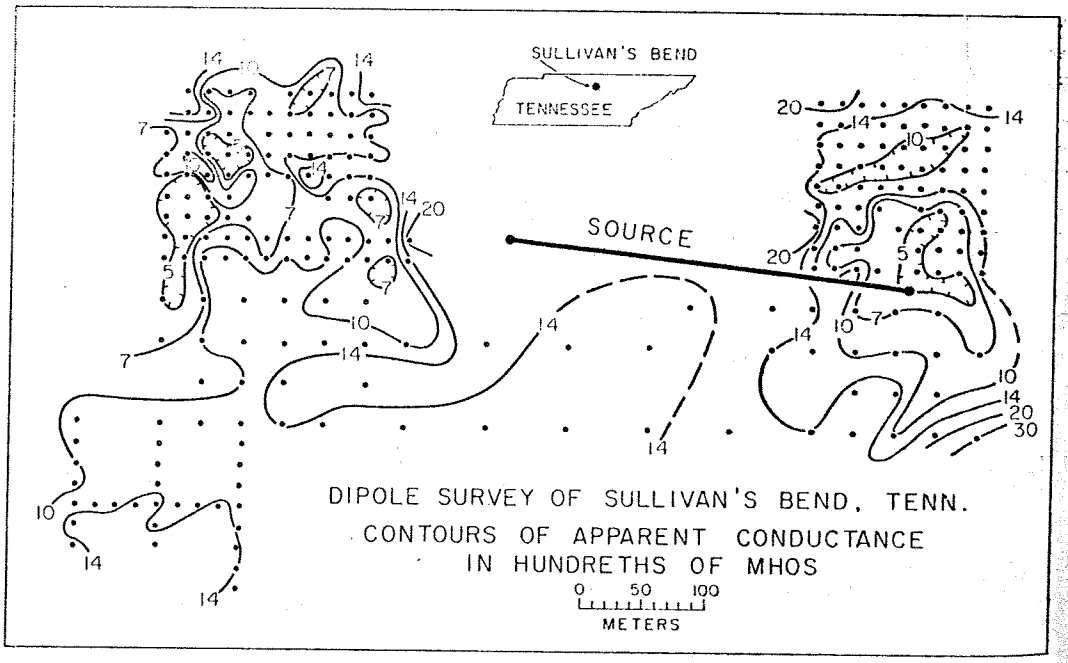

FIG. 22. Contour map of apparent conductance values measured in a survey at Sullivan's Bend, Tenn.

If the assumption that weathered zones retain more water than nonweathered zones is correct, then the regions with low values of conductance (Figure 22) should indicate regions with a thin layer of weathered material, and zones with high conductance should indicate regions with deep weathering. The two areas with high station density, where measurements were made on a grid with a spacing of 15 m, are the proposed locations for structures. These are both areas of low conductance, in the range from .05 to .07 mho, indicating that these are also areas with a thin weathered veneer on bedrock. To the south, the conductance is generally higher, in the range from .10 to .15 mho; in these areas, it is to be expected that the weathered layer is somewhat thicker. There are several small areas with conductance of .20 mho or higher; the small size and large contrast suggests these are locations for locally deep weathering such as a sinkhole.

Conductance depends on both the thickness of the surface layer and its resistivity; a change in either the resistivity or thickness of the surface layer can cause a change in the conductance as mapped in Figure 22. It is sometimes desired to convert conductance values to estimates of the depth to bedrock, as when shallow soundings are used to determine the areal variation of the resistivity in the bedrock. The conversion from conductance is simple but can be made most easily with the nomograph shown in Figure 23. A logical step in the application of resistivity methods to engineering site evaluations would be to carry out a number of shallow resistivity soundings to establish the resistivity of the surface layer at various locations, and then use the values of conductance (as in Figure 22) to determine the probable depth to bedrock.

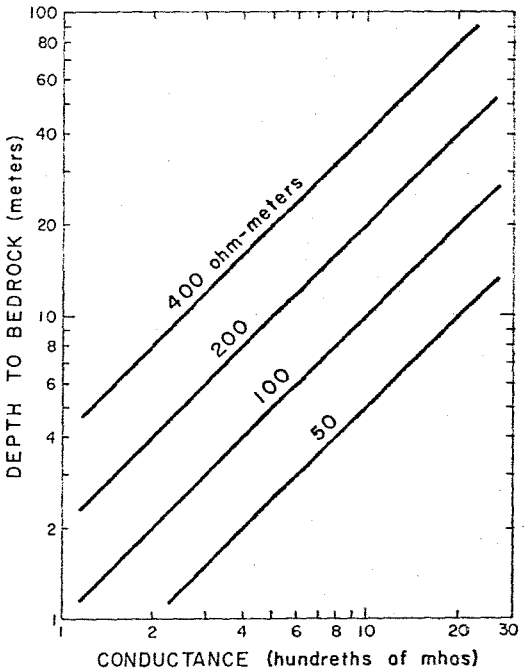

FIG. 23. Nomograph for converting conductance values to depths when surface-layer resistivity is known.

EVALUATION OF DIPOLE MAPPING AS AN EXPLORATION TOOL

Field experience with the dipole mapping method, obtained over the past several years, has caused us to develop a deep appreciation for the merits of the method. The ease with which the method may be used in rugged terrain is a special advantage. Because the source bipole can be located anywhere within range of a target, it is usually possible to locate the source near a road or other area with easy access. Also, because only one source is needed for a large number of measurements, time may be spent efficiently in making certain that the source is well grounded. Existing ground contacts such as metal culverts or well casings are often available, though in some cases it may be necessary to drill shallow wells for electrodes.

Receiving equipment is light, weighing only a few pounds, so measurements may be made in areas with the most difficult access. A secondary advantage of this aspect of the instrumentation is that measurements may be made unobtrusively, at least in some areas well away from the source bipole.

Despite the logistic simplicity of the dipole mapping method, it is not universally reliable, and other, more detailed, studies must usually be carried out in order to define an anomaly adequately. The dipole mapping results provide little information on the depth extent of an anomaly, and resistivity sounding methods are ordinarily needed to complete a model of the subsurface structure.

A further difficulty with the dipole mapping method is that, with a single bipole source, attractive though false resistivity patterns may

appear along the edges of dikes or faults separating regions with markedly different resistivities. As a consequence, it is necessary in anomalous areas to use bipole sources located at different viewing points from the anomaly. If the anomaly persists, it is reasonable to expect that it is real.

ACKNOWLEDGMENTS

The authors are pleased to thank the following for their permission to publish information: Anaconda Copper Co., Indonesian Directorate for Power and Electricity, the Agency for International Development, and the Tennessee Valley Authority.

REFERENCES

Alpin, L. M., 1966, The theory of dipole sounding, *in* Dipole methods for measuring earth conductivity: Consult. Bureau, New York, p. 1–60.

Furgerson, Robert B., 1970, A controlled-source telluric current technique and its application to structural investigations: M.Sc. thesis, Colorado School of Mines.

Furgerson, R. B., and Keller, G. V., 1974, Computed dipole resistivity effects for an earth model with vertical and lateral contrasts in resistivity: Off. Naval Res. Rep. of Investigations, Colorado School of Mines.

Hall, W. E., and MacKevett, E. M., 1962, Geology and ore deposits of the Darwin Quadrangle, Inyo County, California: U.S.G.S. prof. paper 368.

Heiland, C. A., 1940, Geophysical exploration: New York, Prentice-Hall, 1013 p.

Keller, G. V., 1966, Dipole method for deep resistivity studies: Geophysics, v. 31, no. 6, p. 1105–1122.

Keller, G. V., and Frischknecht, F. C., 1966, Electrical methods in geophysical prospecting: Oxford, Pergamon Press, 519 p.

Lee, C. Y., 1973, The dipping layer problem in resistivity: M.Sc. thesis, Colorado School of Mines.

Maeda, Katsuro, 1955, Apparent resistivity for dipping beds: Geophysics, v. 20, p. 123–139.

Meinardus, H. A., 1967, The kernal function in direct-current resistivity sounding: Ph.D. thesis, Colorado School of Mines.

Muffler, L. J. P., 1970, Geothermal potential of the Dieng Mountains, central Java, Indonesia: U.S.G.S. open file rep., Indonesia Investigations, (IR)IND-3.

Risk, G. F., Macdonald, W. J. P., and Dawson, G. B., 1970, D. C. Resistivity surveys of the Broadlands Geothermal Region, New Zealand: Geothermics, v. 2, pt. 1, p. 287–294.

Roman, I., 1959, An image analysis of multiple-layer resistivity problems: Geophysics, v. 24, no. 3, p. 485–509.

Skal'skaya, I. P., 1948, The field of an electrical point source placed over an inclined layer on the earth's surface (in Russian): Akad. Nauk. SSSR Zhur. Tekh. Fiz., v. 18, no. 10, p. 1242–1254.

Tazieff, H., Marinelli, G., and Gorshkov, G. S., 1966, Indonesia volcanological mission (Nov. 1964 to Jan. 1965): Prelim. rep., Paris, UNESCO, WS/0566.58 AVS, 25 p.

Umbgrove, J. H. F., 1930, Het ontstaan van Ret Diengslateau: Leidsche Geologische Mededeelingen, Deel III. Rijks-Geologisch-Mineralogisch Museum te Leiden, p. 131–150 (in Dutch).

Van Nostrand, R. G., and Cook, K. L., 1966, Interpretation of resistivity data: U.S.G.S. Bull. 499, 310 p.

van Padang, M. Neumann, 1936, Het Dieng geberte: De Tropische Natuur, frg. 25, p. 27–36 (in Dutch).

Vedrintsev, G. A., 1966, Theory of electric sounding in a medium with lateral discontinuities, *in* Dipole methods for measuring earth conductivity: Consult. Bureau, New York, p. 115–146.

Zen, M. T., 1971, Geothermal system of the Dieng-Batur volcanic complex: Proc. Inst. Tech. Bandung, v. 6, no. 1, p. 23–38.